Hydrological Research Letters **18**(4), 87–94 (2024)
Published online in J-STAGE (www.jstage.jst.go.jp/browse/hrl). DOI: 10.3178/hrl.18.87

Evaluation and selection of a set of CMIP6 GCMs for water resource modeling in the poorly gauged complex terrain of the Tana River basin in Kenya

Daniel Mwendwa Wambua[1,2], Hiroaki Somura[1] and Toshitsugu Moroizumi[1]
[1]*Graduate School of Environmental and Life Science, Okayama University, Japan*
[2]*Department of Soil, Water, and Environmental Engineering, Jomo Kenyatta University of Agriculture and Technology, Kenya*

Abstract:

The Tana River basin is among the least monitored in terms of meteorological data in Kenya. The Kenya Meteorological Department (KMD) provided data on a ten-day timescale, which is not adequate for water resource evaluation. To bridge this data gap, there is a growing need to leverage General Circulation Models (GCMs) and global datasets to assess current and future water resources in this basin. This study focused on evaluating the performance of 19 CMIP6 GCMs concerning precipitation (pr), maximum temperature (tasmax), and minimum temperature (tasmin) for the complex terrain of the Tana River basin. This involved a rigorous process of disaggregating the data provided by the KMD into a daily timescale for downscaling. The GCMs' historical output was prepared using the Climate Data Operator (CDO) in Cygwin. The Kling Gupta Efficiency (KGE) was computed for each variable at three stations: Nyeri (upstream), Kitui (midstream), and Bura (downstream). The KGE results were validated using Taylor statistics. Five GCMs, CMCC-ESM2, MPI-ESM1-2-HR, ACCESS-CM2, NorESM2-MM, and GFDL-ESM4, performed best with a multivariable Multi-station KGE statistic of 0.455–0.511. The outputs from these selected GCMs were subsequently downscaled for later use in assessing the water resources and crop water demand in the basin.

KEYWORDS climate change; adaptation; scenarios; downscaling; disaggregation; temporal

INTRODUCTION

The Tana River basin in Kenya, renowned for its equatorial location, grapples with the complex challenges caused by climate change. The region has experienced an alarming increase in the frequency and severity of extreme weather events, including droughts and floods, while global warming continues to reshape its hydrological landscape (Masson-Delmotte *et al.*, 2021; McCartney *et al.*, 2021). These climate-induced shifts have profound implications for water resources, affecting sectors ranging from agriculture to domestic water supply (Dibaba *et al.*, 2020; Mutua *et al.*, 2018).

Compounding these challenges is Kenya's projected annual population growth of nearly one million people between 2019 and 2050 (Mwaila and Yousif, 2022), which paints a grim picture of the intersection between climate change and dwindling freshwater resources. This situation is particularly acute in the Tana River basin, which is predominantly characterized as an arid and semi-arid area (ASAL). Nonetheless, this region carries significant economic significance for Kenya, supporting irrigation, hydroelectric power generation, and vital water supply needs (The 2030 WRG-Kenya, 2015). The proposed construction of water-impounding structures in the upper Tana, such as the Grand-Falls dam, further complicates the situation by reducing the downstream flows during the dry season.

Addressing these challenges requires a comprehensive assessment of available water resources, both present and future, within the context of climate change. Achieving this objective requires datasets with higher temporal resolution, ideally on a daily basis. However, in regions with limited gauge coverage, such as the Tana River basin (Leauthaud *et al.*, 2013), acquiring extensive and continuous datasets is a challenging endeavor.

Existing meteorological stations in the Tana River basin offer limited data, typically covering precipitation and temperature. This limitation is exacerbated by constraints related to equipment availability, financial resources, temporal coverage, data quality, accessibility, and data-sharing policies. The KMD, responsible for these stations, usually provides data on a monthly timescale, which often suffers from missing data (Gebrechorkos *et al.*, 2019). However, for this study, KMD at least provided ten-day (dekadal) data upon request. These monthly/ten-day data fall short of facilitating a comprehensive water resource analysis or crop water demand calculations for irrigation scheduling. Moreover, these datasets cannot directly support the downscaling of daily GCM outputs (Lai *et al.*, 2022).

To overcome these challenges, we turn to GCMs, which are powerful tools capable of simulating historical and future weather patterns on a global scale (Eyring *et al.*, 2016). Despite their limitations in capturing climatological heterogeneity in terrain complex catchments (TCC), they

Correspondence to: Hiroaki Somura, Graduate School of Environmental and Life Science, Okayama University, 3-1-1 Tsushima-Naka, Kita-ku, Okayama 700-8530, Japan. E-mail: somura@okayama-u.ac.jp

Received 16 November, 2023
Accepted 27 January, 2024
Published online 9 October, 2024

are invaluable for understanding current and future climates, especially in regions with limited meteorological gauges (Farjad *et al.*, 2016; Usman *et al.*, 2022). To address the limitations in capturing climatological heterogeneity, statistical downscaling of the GCMs' outputs to specific weather stations within the basin can help capture the climatic diversity in areas of proximity to each other.

In this context, the recently developed World Climate Research Programme (WCRP) Coupled Model Intercomparison Project 6 (CMIP6) GCMs offer promise. Notably, CMIP6 GCMs have demonstrated improvements, particularly in modeling precipitation, which is attributed to advances in cloud modeling (Eyring *et al.*, 2016). Their output has been instrumental in assessing water resources worldwide (Chen *et al.*, 2020; Hamed *et al.*, 2022; Shiru and Chung, 2021). Nevertheless, the effectiveness of GCMs depends on various factors including their underlying physics and resolution (Bozkurt *et al.*, 2019). GCM outputs are too coarse, with a resolution exceeding 100 kilometers, to be directly employed in impact assessment studies, adaptation planning, and local or regional decision-making processes. Therefore, downscaling is imperative to enhance spatial resolution and minimize biases before using climate projections for impact assessment and adaptation planning (Gebrechorkos *et al.*, 2019; Keller *et al.*, 2022). The limited ground observations still play a pivotal role in downscaling the GCM outputs.

Our study focuses on the Tana River basin, with the primary objective of evaluating and selecting a suitable GCM ensemble from a set of 19 CMIP6 GCMs using key performance indicators like KGE and Taylor statistics. Subsequently, we downscaled the chosen GCMs using the disaggregated KMD precipitation and temperature datasets (Text S1). These downscaled datasets will be employed in future studies to evaluate water resources and crop water demand, thereby providing essential insights for farmers and policymakers in their efforts to build resilience in the face of a changing climate. By leveraging global datasets, ground-based observations, and GCM outputs, we aim to comprehensively assess the impact of climate change on water resources and crop water demand.

MATERIALS AND METHODS

Study area

Figure 1 shows the delineated Tana River basin with the three altitude zones and the weather stations used in this study for selecting the GCMs. The basin is located between latitudes 0.5°N/3.0°S and longitudes 36.5°E/41.0°E. The Tana River basin, one of the largest basins in Kenya, holds significant importance as it serves as a vital source of water for major irrigation schemes and hydropower generation across the seven forks dams. Moreover, water is transferred from the basin for domestic and industrial uses in Kenya's capital, Nairobi City. The altitude rises from 0 m at sea level to 5199 m at the peak of Mount Kenya. Rainfall increases with altitude, with most of the precipitation received in the smaller part of the upper basin, while the rest of the basin receives less than 500 mm of annual precipitation.

Conversely, temperature decreases with altitude with the coastal and low-lying areas, experiencing temperatures above 35°C during the hottest months. This makes evapotranspiration a major form of water loss from the basin, with notable streamflow declines between the Garissa and Garsen River gauging stations (Leauthaud *et al.*, 2013). Consequently, high temperatures lead to increased crop water demand and reduced water storage in the channels and reservoirs.

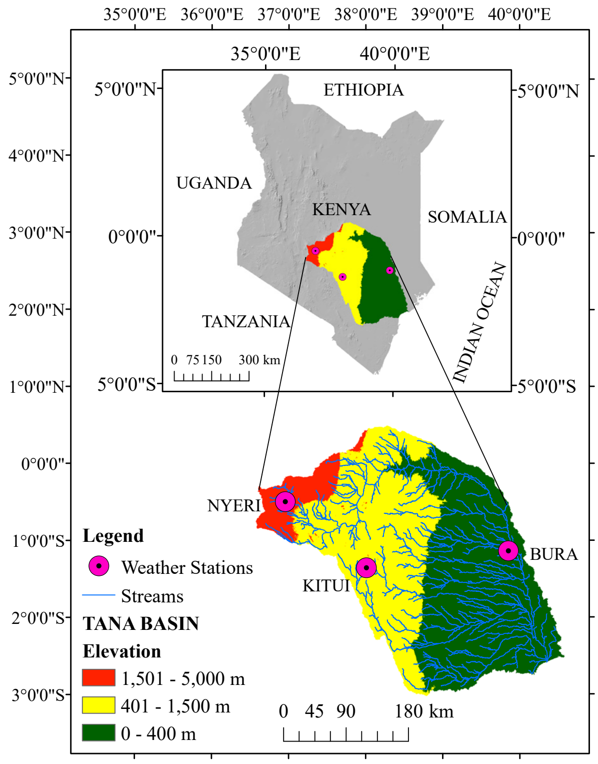

Figure 1. Study area map

The diversity in altitude, weather, and soil contributes to a rather diverse set of climates and vegetation, which leads to distinct climates within areas of proximity to each other.

Data and software

Figure 2 shows the overview of the methodological approach. In this study, 19 CMIP6 GCMs were selected and accessed at https://esgf.llnl.gov/nodes.html (O'Neill *et al.*, 2016). Table SI shows the set of 19 GCMs. The selection of the 19 GCMs was based on: (a) availability of projections of three main climate variables: precipitation (pr), maximum temperature (tasmax), and minimum temperature (tasmin), and (b) availability of historical and future projections for SSP126, SSP245, and SSP585. The SSP126 represents a world where there is rapid, sustainable development with low population growth, increased resource efficiency, and a focus on environmental stewardship. The SSP245 represents a future where the world follows a moderate path, balancing economic, social, and environmental objectives. It assumes population growth, moderate technological progress, and a continuation of historical development trends. Lastly, the SSP585 envisions a future heavily dependent on fossil fuels, with rapid and unconstrained economic growth, high population growth,

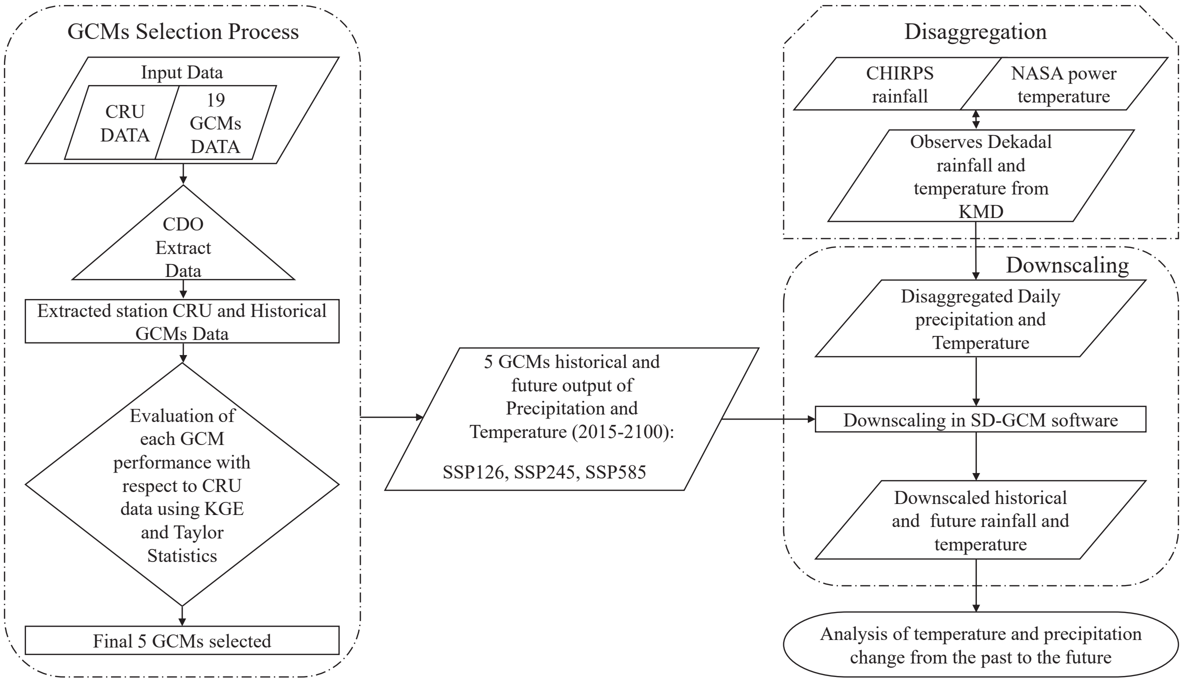

Figure 2. An overview of the methodological approach. CRU = Climate Research Unit, GCMs = General Circulation Models, CDO = Climate Data Operator, KGE = Kling Gupta Efficiency, CHIRPs = Climate Hazard Infrared Precipitation with Stations, KMD = Kenya Meteorological Department, SD GCM = a GCMs output statistical downscaling software

and limited environmental regulation. It is associated with the highest greenhouse gas emissions and limited efforts for climate change mitigation. The three SSP scenarios were selected to represent three possible futures of (1) sustainable development, (2) business as usual future, and (3) an unsustainable future. Selecting the three SSP scenarios enabled the evaluation of the wide range (best-case to a worst-case scenario) of possible futures which are associated with great uncertainty. After downloading, data processing was performed using the Climate Data Operator (CDO) in Cygwin. Finally, the extraction of each variable for each station, namely Nyeri, Kitui, and Bura, was performed using CDO and used to calculate the KGE and Taylor statistics.

The three stations, Nyeri, Kitui, and Bura, were created to make use of the Climate Research Unit (CRU) and Climate Hazard Infrared Precipitation with Stations (CHIRPS) datasets for the evaluation of GCMs. This is because the existing weather stations were mired with many missing data points and were not well distributed across the entire basin. These stations are different from the stations used in downscaling, except for Nyeri station. Text S2 provides further description of the KGE and Taylor statistics used in this study.

Downscaling

In this study, the SD GCM downscaling software designed by Agrimetsoft® research company was considered. Full documentation about SD GCM can be found at https://agrimetsoft.com/SD-GCM.aspx (AgriMetsoft, 2018). The weather stations used for downscaling are shown in Figure S1. In the analysis of the downscaled data, the future projections of 2015–2099 were split into three time periods of near future (2026–2050), mid future (2051–2075) and far future (2076–2099) to help in the visualization of the state of the future climate in those three distinct future times as one moves from the present to the end of the century.

RESULTS

GCMs selection

Table SII shows the KGE statistics for pr and tasmax, while Table SIII shows the KGE statistics for tasmin and average KGE for tasmin, tasmax, and pr for all stations for the 19 GCMs and their multi-model ensemble (MME). For pr, the GCMs performed the best in the midstream, followed by upstream, and poorest in the Bura station downstream. GFDL-ESM4 (Krasting *et al.*, 2018) was the best performing GCM with a KGE of 0.785 at Kitui Station. Conversely, IPSL-CM6A-LR (Boucher *et al.*, 2018) was the worst performing GCM, with a KGE of –1.965 at the Bura station downstream of the basin. The GCMs seemed to best predict pr in the midstream of the basin, which receives an average pr of 600–900 mm/year.

All the GCMs, except for KIOST-ESM (Kim *et al.*, 2019), showed a good capability to predict tasmax in both Kitui and Bura, respectively, in the midstream and downstream. The GCMs prediction of temperature in the hilly and mountainous upstream areas was relatively poorer than that in the downstream areas. In the tasmax category, MPI-ESM1-2-HR (Jungclaus *et al.*, 2019) performed best with a KGE of 0.885 at the Bura station, whereas KIOST-ESM (Kim *et al.*, 2019) performed the poorest with a KGE of −0.576 at the Nyeri station.

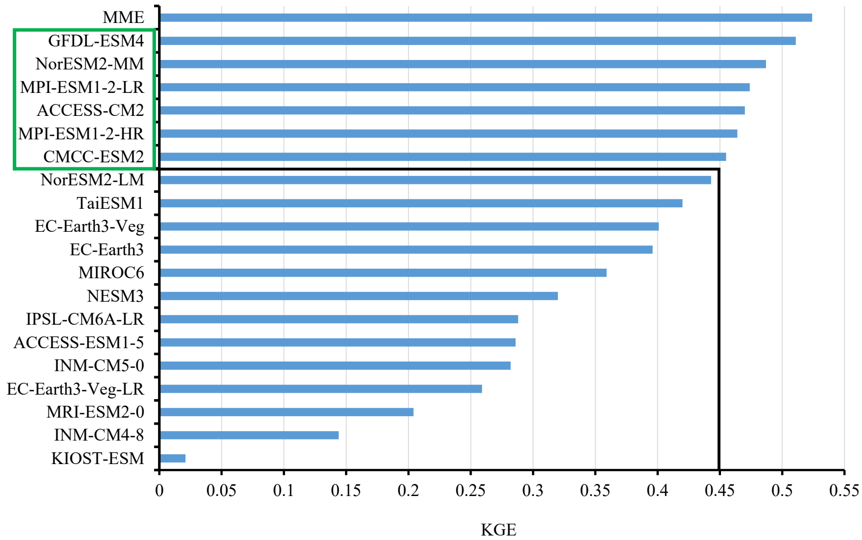

Figure 3. Multi-variable-multi-location KGE per GCM. MME = Multi-Model Ensemble, KGE = Kling Gupta Efficiency

Like tasmax, the GCMs predicted tasmin better at the Kitui and Bura stations in the midstream and downstream, respectively, compared to Nyeri in the upstream of the basin. ACCESS-ESM1-5 (Ziehn *et al.*, 2019) GCM at the Kitui station performed best for tasmin with a KGE of 0.932, while NESM3 (Cao and Wang, 2019) at the Nyeri station performed poorest with a KGE of –0.699.

The KGE statistics for the three variables (pr, tasmin, and tasmax) were further aggregated into one KGE by averaging across the three variables. This KGE is referred to as the multi-variable, multi-location KGE per GCM. The KGE statistics were averaged across locations and variables to assess each GCM's performance across the considered variables and elevations. This holistic approach evaluates how well a GCM can simulate the basin's future weather for all variables and locations combined. This differs from the common practice of evaluating GCMs for individual variables and locations, which can result in different GCM sets for different variables. Selecting a GCM separately for each variable and elevation may hinder obtaining a suitable ensemble for subsequent studies, like those related to hydrology and crop water demand. By ranking the KGEs from largest to smallest, the best GCMs were obtained for further study, as shown in Figure 3. Figure 4 shows the Taylor diagram for the 19 GCMs and their MME for all stations and variables combined. GCMs 18, 13, 14, 1, 3, and 7 corresponding to NorESM2-MM (Bentsen *et al.*, 2019a), MPI-ESM1-2-HR (Jungclaus *et al.*, 2019), GFDL-ESM4 (Krasting *et al.*, 2018), MPI-ESM1-2-LR (Wieners *et al.*, 2019), CMCC-ESM2 (Lovato *et al.*, 2021a), and ACCESS-CM2 (Dix *et al.*, 2019a), respectively, were selected for the Taylor statistic. The same set of GCMs was realized in the two methods, although with different rankings for both the KGE and Taylor methods as shown in Table SIV and Table SV respectively. Text S3 provides more details on the KGE and Taylor statistics.

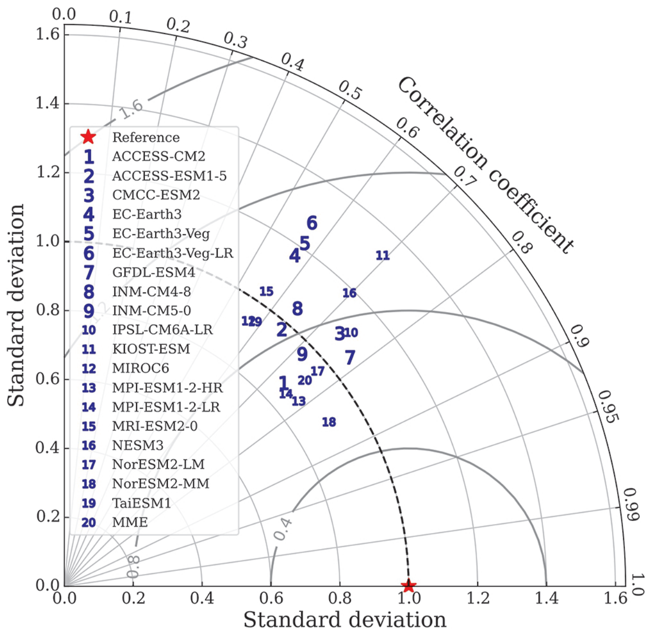

Figure 4. Taylor diagram for the set of 19 GCMs across all stations and all variables with reference to the observed point. MME = Multi-Model Ensemble

Evaluation of the downscaled historical and future projections of the selected GCMs

On a daily scale, the selected GCMs slightly overestimated the number of wet days (Figure S2) and underestimated the maximum pr (Figure S3). Figure S4 shows the annual pr at each station for the observed and GCMs' MME for the historical period (1981–2014). The MME of the downscaled GCMs fairly replicated the observed annual and seasonal pr. There is an observed increase in pr for all stations in the basin for SSP126. The MME of the downscaled GCMs showed a gradual increase in pr from the near future (2026–2050) to the far future (2076–2099) under SSP126 at all stations (Figure 5). The highest increase was observed in September, October, and November (SON). Similar trends were observed for SSP245 and SSP585.

For tasmax, the MME of the GCMs fairly predicted the average and maximum daily tasmax as well as the extreme hot (> 30°C) days for each station considered. The level of prediction for tasmax was better than that for pr and tasmin (Yang *et al.*, 2021). On annual and seasonal scales, the MME of the GCMs fairly predicted the average and maximum tasmax (Figure S5 and Figure S6). The highest increase in tasmax was observed in June, July, and August (JJA) (Figure 6). The MME of the downscaled GCMs showed a gradual increase in tasmax from the near future to the far future under SSP126 at all stations (Figure S7). Similar trends were observed for tasmax for SSP245 and SSP585.

The GCMs' MME fairly predicted the average and minimum tasmin. However, MME overestimated the extreme cold (< 10°C) days for most stations. On annual and seasonal scales, the MME of the GCMs predicted the average and minimum tasmin well. The highest increases in tasmin were observed in January, February, and March (JFM), with the highest average increase recorded as 3.7°C at Nyeri station (Figure S8). The downscaled GCMs MME showed a gradual increase in tasmin from the near future to the far future under SSP126 at all stations (Figure S9). Similar trends were observed for SSP245 and SSP585 for tasmin. Further explanation of the evaluation of future scenarios is provided in Text S4.

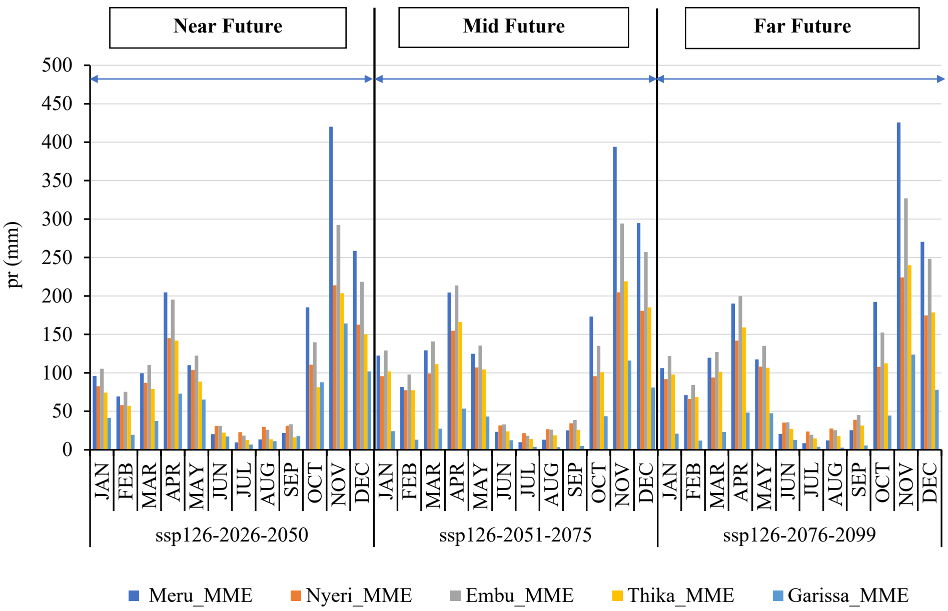

Figure 5. Multiyear monthly average total precipitation for SSP126. MME = Multi-Model Ensemble

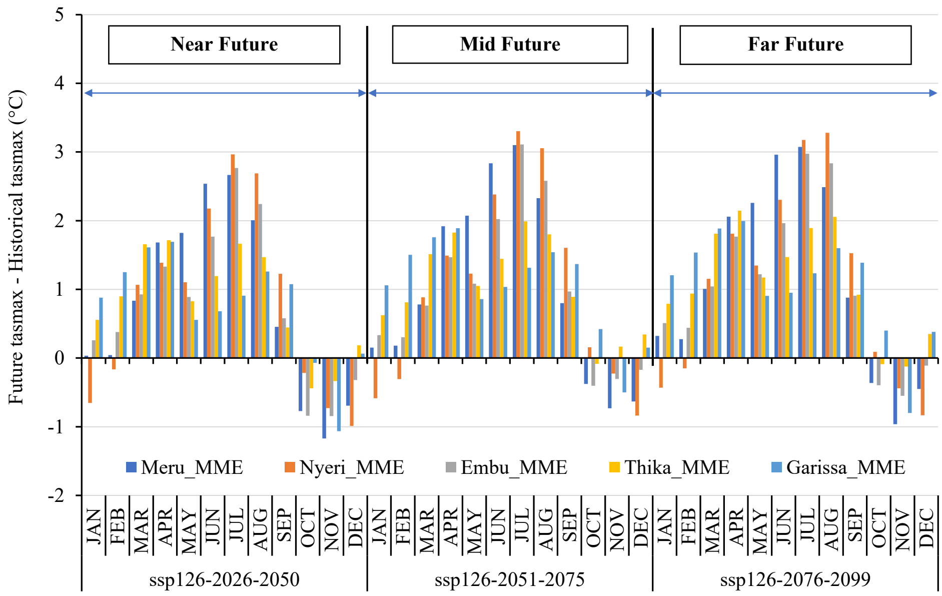

Figure 6. Multiyear monthly average tasmax difference from observed for SSP126. MME = Multi-Model Ensemble

DISCUSSION

The process of selecting GCMs for water resource evaluation can be particularly challenging, especially in poorly gauged regions. Hamed *et al.* (2022) highlighted the difficulty in selecting GCMs for future climate predictions. Our study used a combination of KGE and Taylor statistics to identify a suitable set of GCMs for water resource and crop water demand assessments, despite the lack of a universally accepted methodology for selecting GCMs.

Our study found that CMIP6 GCMs effectively predicted pr, tasmax, and tasmin. pr was the least accurate among the three, which aligns with findings of Lu *et al.* (2022) and Wang *et al.* (2022). Improved pr modeling, especially in cloud modeling, as suggested by Ayugi *et al.* (2021) and Eyring *et al.* (2016), contributes to this enhanced capability. The GCMs also exhibited varying predictive abilities for the three variables across different areas of the TCC.

The GCMs showed better predictions for tasmax and tasmin in the arid and semi-arid midstream and downstream regions than in the humid upstream regions. pr prediction was highest in the midstream region, contrary to predictions for upstream and downstream regions. GCM performance varied for different weather variables and locations, as found by Iqbal *et al.* (2021). To minimize bias in GCM selection and accurately predict pr, tasmax, and tasmin across the three locations of the TCC, a multivariable multi-location approach was adopted.

Geographical location and terrain complexity may explain discrepancies in optimal GCMs, as suggested by Shiru and Chung (2021). Leveraging global datasets, ground-based observations, and GCM outputs can help address the need for precise and high-resolution climate data in under-gauged regions.

Unable to access daily data, GCMs were downscaled using disaggregated KMD data, a time-consuming process due to the inability to directly use KMD data for downscaling GCM outputs. The downscaling successfully removed biases in coarse GCMs, resulting in station-based time-series data for selected stations in historical and future scenarios. Future scenarios analysis showed increased wetness in wetter areas of the basin and a shift in annual precipitation distribution. This may lead to increased flooding in the lower parts of the basin due to more intense precipitation. The October, November, and December (OND) season is predicted to be wetter than the March, April, and May (MAM) season, potentially impacting crop production during MAM due to high temperatures that lead to increased evapotranspiration.

The study observed higher temperature increases in the cooler parts of the basin, especially during JJA – a finding consistent with Shao *et al.* (2023). The shift in precipitation and increased temperature during cooler periods may also worsen water scarcity and hillside erosion during heavy precipitation, consistent with Yang *et al.* (2021).

CONCLUSION

An ensemble of 19 GCMs was used to evaluate water resources and water demand in the Tana River basin. Five GCMs, NorESM2-MM, MPI-ESM1-2-HR, GFDL-ESM4, CMCC-ESM2, and ACCESS-CM2, were selected based on Taylor and KGE statistics. These GCMs captured the historical climate of the basin on different scales, indicating their suitability for evaluating water resources and crop water demand in the absence of measured weather data. Future forecasts showed gradually increasing temperatures and precipitation with intra-annual variations, which could lead to increased flooding and crop failure during dry periods.

ACKNOWLEDGMENTS

The authors are grateful to JICA for providing financial support during the doctoral program for the first author in Japan. Special thanks are expressed to the climate modeling groups (listed in Table SI) for producing and making available their model outputs.

SUPPLEMENTS

Text S1. Observed data preparation and downscaling
Text S2. KGE and Taylor statistics description
Text S3. Further discussion on KGE statistics results
Text S4. Evaluation of the downscaled GCMs future scenario for the selected GCMs
Figure S1. Study area weather stations used in downscaling CMIP6 GCMs
Figure S2. Long term number of wet days for observed data and downscaled GCMs MME for 1981–2014
Figure S3. Long term historical maximum daily precipitation for observed data and downscaled GCMs MME for 1981–2014
Figure S4. Annual observed and GCMs MME pr for 1981–2014
Figure S5. Long term annual tasmax statistics for observed and downscaled GCM MME for 1981–2014
Figure S6. Long term seasonal average tasmax for observed and downscaled GCM MME for 1981–2014
Figure S7. Multiyear monthly average tasmax for SSP126
Figure S8. Multiyear monthly average tasmin difference from observed for SSP126
Figure S9. Multiyear monthly average tasmin for SSP126
Table SI. List of the 19 CMIP6 GCMs selected for suitability evaluation for this study
Table SII. KGE statistics for pr and tasmax at different stations
Table SIII. KGE statistics for tasmin, average KGE for precipitation, tasmax and tasmin
Table SIV. List of GCMs selected based on KGE statistics
Table SV. List of GCMs selected based on Taylor statistics

REFERENCES

AgriMetSoft. 2018. SD-GCM Tool [Computer software]. https://agrimetsoft.com/SD-GCM.aspx. Last access April 20, 2023.

Ayugi B, Zhihong J, Zhu H, Ngoma H, Babaousmail H, Rizwan K, Dike V. 2021. Comparison of CMIP6 and CMIP5 models in simulating mean and extreme precipitation over East

Africa. *International Journal of Climatology* **41**: 6474–6496. DOI: 10.1002/joc.7207.

Bentsen M, Olivè DJL, Seland Ø, Toniazzo T, Gjermundsen A, Graff LS, Debernard JB, Gupta AK, He Y, Kirkevåg A, Schwinger J, Tjiputra J, Aas KS, Bethke I, Fan Y, Griesfeller J, Grini A, Guo C, Ilicak M, Karset IHH, Landgren OA, Liakka J, Moseid KO, Nummelin A, Spensberger C, Tang H, Zhang Z, Heinze C, Iversen T, Schulz M. 2019a. NCC NorESM2-MM model output prepared for CMIP6 CMIP historical. Version 20220607. *Earth System Grid Federation*. DOI: 10.22033/ESGF/CMIP6.8040.

Boucher O, Denvil S, Levavasseur G, Cozic A, Caubel A, Foujols MA, Meurdesoif Y, Cadule P, Devilliers M, Ghattas J, Lebas N, Lurton T, Mellul L, Musat I, Mignot J, Cheruy F. 2018. IPSL IPSL-CM6A-LR model output prepared for CMIP6 CMIP historical. Version 20220607. *Earth System Grid Federation*. DOI: 10.22033/ESGF/CMIP6.5195.

Bozkurt D, Rojas M, Boisier JP, Rondanelli R, Garreaud R, Gallardo L. 2019. Dynamical downscaling over the complex terrain of southwest South America: present climate conditions and added value analysis. *Climate Dynamics* **53**: 6745–6767. DOI: 10.1007/s00382-019-04959-y.

Cao J, Wang B. 2019. NUIST NESMv3 model output prepared for CMIP6 CMIP historical. Version 20220607. *Earth System Grid Federation*. DOI: 10.22033/ESGF/CMIP6.8769.

Chen Z, Zhou T, Zhang L, Chen X, Zhang W, Jiang J. 2020. Global land monsoon precipitation changes in CMIP6 projections. *Geophysical Research Letters* **47**: e2019GL086902. DOI: 10.1029/2019GL086902.

Dibaba WT, Demissie TA, Miegel K. 2020. Watershed hydrological response to combined land use/land cover and climate change in highland Ethiopia: finchaa catchment. *Water* **12**: 1801. DOI: 10.3390/w12061801.

Dix M, Bi D, Dobrohotoff P, Fiedler R, Harman I, Law R, Mackallah C, Marsland S, O'Farrell S, Rashid H, Srbinovsky J, Sullivan A, Trenham C, Vohralik P, Watterson I, Williams G, Woodhouse M, Bodman R, Dias FB, Domingues CM, Hannah N, Heerdegen A, Savita A, Wales S, Allen C, Druken K, Evans B, Richards C, Ridzwan SM, Roberts D, Smillie J, Snow K, Ward M, Yang R. 2019a. CSIRO-ARCCSS ACCESS-CM2 model output prepared for CMIP6 CMIP historical. Version 20220607. *Earth System Grid Federation*. DOI: 10.22033/ESGF/CMIP6.4271.

Eyring V, Bony S, Meehl GA, Senior CA, Stevens B, Stouffer RJ, Taylor KE. 2016. Overview of the coupled model intercomparison project phase 6 (CMIP6) experimental design and organization. *Geoscientific Model Development* **9**: 1937–1958. DOI: 10.5194/gmd-9-1937-2016.

Farjad B, Gupta A, Marceau DJ. 2016. Annual and seasonal variations of hydrological processes under climate change scenarios in two sub-catchments of a complex watershed. *Water Resources Management* **30**: 2851–2865. DOI: 10.1007/s11269-016-1329-3.

Gebrechorkos SH, Hülsmann S, Bernhofer C. 2019. Statistically downscaled climate dataset for East Africa. *Scientific Data* **6**: 31. DOI: 10.1038/s41597-019-0038-1.

Hamed MM, Nashwan MS, Shahid S. 2022. A novel selection method of CMIP6 GCMs for robust climate projection. *International Journal of Climatology* **42**: 4258–4272. DOI: 10.1002/joc.7461.

Iqbal Z, Shahid S, Ahmed K, Ismail T, Ziarh GF, Chung ES, Wang X. 2021. Evaluation of CMIP6 GCM rainfall in mainland Southeast Asia. *Atmospheric Research* **254**: 105525. DOI: 10.1016/j.atmosres.2021.105525.

Jungclaus J, Bittner M, Wieners KH, Wachsmann F, Schupfner M, Legutke S, Giorgetta M, Reick C, Gayler V, Haak H, de Vrese P, Raddatz T, Esch M, Mauritsen T, von Storch JS, Behrens J, Brovkin V, Claussen M, Crueger T, Fast I, Fiedler S, Hagemann S, Hohenegger C, Jahns T, Kloster S, Kinne S, Lasslop G, Kornblueh L, Marotzke J, Matei D, Meraner K, Mikolajewicz U, Modali K, Müller W, Nabel J, Notz D, Peters-von Gehlen K, Pincus R, Pohlmann H, Pongratz J, Rast S, Schmidt H, Schnur R, Schulzweida U, Six K, Stevens B, Voigt A, Roeckner E. 2019. MPI-M MPI-ESM1.2-HR model output prepared for CMIP6 CMIP historical. Version 20220607. *Earth System Grid Federation*. DOI: 10.22033/ESGF/CMIP6.6594.

Keller AA, Garner KL, Rao N, Knipping E, Thomas J. 2022. Downscaling approaches of climate change projections for watershed modeling: review of theoretical and practical considerations. *PLOS Water* **1**: 0000046. DOI: 10.1371/journal.pwat.0000046.

Kim YH, Noh Y, Kim D, Lee MI, Lee HJ, Kim SY, Kim D. 2019. KIOST KIOST-ESM model output prepared for CMIP6 CMIP historical. Version 20220607. *Earth System Grid Federation*. DOI: 10.22033/ESGF/CMIP6.5296.

Krasting JP, John JG, Blanton C, McHugh C, Nikonov S, Radhakrishnan A, Rand K, Zadeh NT, Balaji V, Durachta J, Dupuis C, Menzel R, Robinson T, Underwood S, Vahlenkamp H, Dunne KA, Gauthier PPG, Ginoux P, Griffies SM, Hallberg R, Harrison M, Hurlin W, Malyshev S, Naik V, Paulot F, Paynter DJ, Ploshay J, Reichl BG, Schwarzkopf DM, Seman CJ, Silvers L, Wyman B, Zeng Y, Adcroft A, Dunne JP, Dussin R, Guo H, He J, Held IM, Horowitz LW, Lin P, Milly PCD, Shevliakova E, Stock C, Winton M, Wittenberg AT, Xie Y, Zhao M. 2018. NOAA-GFDL GFDL-ESM4 model output prepared for CMIP6 CMIP historical. Version 20220607. *Earth System Grid Federation*. DOI: 10.22033/ESGF/CMIP6.8597.

Lai C, Chen X, Zhong R, Wang Z. 2022. Implication of climate variable selections on the uncertainty of reference crop evapotranspiration projections propagated from climate variables projections under climate change. *Agricultural Water Management* **259**: 107273. DOI: 10.1016/j.agwat.2021.107273.

Leauthaud C, Belaud G, Duvail S, Moussa R, Grünberger O, Albergel J. 2013. Characterizing floods in the poorly gauged wetlands of the Tana River Delta, Kenya, using a water balance model and satellite data. *Hydrology and Earth System Sciences* **17**: 3059–3075. DOI: 10.5194/hess-17-3059-2013.

Lovato T, Peano D, Butenschön M. 2021a. CMCC CMCC-ESM2 model output prepared for CMIP6 CMIP historical. Version 20220607. *Earth System Grid Federation*. DOI: 10.22033/ESGF/CMIP6.13195.

Lu K, Arshad M, Ma X, Ullah I, Wang J, Shao W. 2022. Evaluating observed and future spatiotemporal changes in precipitation and temperature across China based on CMIP6-GCMs. *International Journal of Climatology* **42**: 7703–7729. DOI: 10.1002/joc.7673.

Masson-Delmotte VP, Zhai P, Pirani SL, Connors C, Péan S, Berger N, Scheel Monteiro PM. 2021. IPCC, 2021: SPM – Summary for policymakers. in: Climate change 2021: the physical science basis. contribution of working group I to the sixth assessment report of the intergovernmental panel on climate change. Cambridge University Press, Cambridge, UK and NY, USA; 1–32. DOI: 10.1017/9781009157896.001.

McCartney S, Mehta A, Ruane A, Bader D. 2021. Introduction to NASA Resources for Climate Change Applications. NASA Applied Remote Sensing Training Program (ARSET). https://appliedsciences.nasa.gov/join-mission/training/english/arset-introduction-nasa-resources-climate-change-applications. Last access March 30, 2022.

Mutua BM, Wambua RM, Raude JM. 2018. Drought forecasting under climate change scenarios using artificial neural networks for sustainable water resources management in upper Tana river basin, Kenya. *PAUWES Research-2-Practice Forum* **2018**: 1–6. DOI: 10.2139/ssrn.3210560.

Mwaila MM, Yousif MT. 2022. Kenya's ageing population: current and future prospects. *World Journal of Advanced Research and Reviews* **16**: 598–610. DOI: 10.30574/wjarr.2022.16.2.1161.

O'Neill BC, Tebaldi C, van Vuuren DP, Eyring V, Friedlingstein P, Hurtt G, Knutti R, Kriegler E, Lamarque JF, Lowe J, Meehl GA, Moss R, Riahi K, Sanderson BM. 2016. The Scenario Model Intercomparison Project (ScenarioMIP) for CMIP6. *Geoscientific Model Development* **9**: 3461–3482. DOI: 10.5194/gmd-9-3461-2016.

Shao X, Zhang Y, Ma N, Zhang X, Tian J, Liu C. 2023. Flood increase and drought mitigation under a warming climate in the Southern Tibetan Plateau. *Journal of Geophysical Research: Atmospheres* **128**: e2022JD037835. DOI: 10.1029/2022JD037835.

Shiru MS, Chung ES. 2021. Performance evaluation of CMIP6 global climate models for selecting models for climate projection over Nigeria. *Theoretical and Applied Climatology* **146**: 599–615. DOI: 10.1007/s00704-021-03746-2.

The 2030 Water Resource Group (WRG)-Kenya. 2015. Water Resources in Kenya: Closing the Gap. A *Briefing note*. https://2030wrg.org/wp-content/uploads/2015/05/Kenya-Hydro-Economic-Briefing-Note_May2015.pdf. Last access March 30, 2022.

Usman M, Manzanas R, Ndehedehe CE, Ahmad B, Adeyeri OE, Dudzai C. 2022. On the benefits of bias correction techniques for streamflow simulation in complex terrain catchments: a case-study for the chitral river basin in Pakistan. *Hydrology* **9**: 188. DOI: 10.3390/hydrology9110188.

Wang L, Li Y, Li M, Li L, Liu F, Li Liu D, Pulatov B. 2022. Projection of precipitation extremes in China's mainland based on the statistical downscaled data from 27 GCMs in CMIP6. *Atmospheric Research* **280**: 106462. DOI: 10.1016/j.atmosres.2022.106462.

Wieners KH, Giorgetta M, Jungclaus J, Reick C, Esch M, Bittner M, Legutke S, Schupfner M, Wachsmann F, Gayler V, Haak H, de Vrese P, Raddatz T, Mauritsen T, von Storch JS, Behrens J, Brovkin V, Claussen M, Crueger T, Fast I, Fiedler S, Hagemann S, Hohenegger C, Jahns T, Kloster S, Kinne S, Lasslop G, Kornblueh L, Marotzke J, Matei D, Meraner K, Mikolajewicz U, Modali K, Müller W, Nabel J, Notz D, Peters-von Gehlen K, Pincus R, Pohlmann H, Pongratz J, Rast S, Schmidt H, Schnur R, Schulzweida U, Six K, Stevens B, Voigt A, Roeckner E. 2019. MPI-M MPI-ESM1.2-LR model output prepared for CMIP6 CMIP historical. Version 20220607. *Earth System Grid Federation*. DOI: 10.22033/ESGF/CMIP6.6595.

Yang X, Zhou B, Xu Y, Han Z. 2021. CMIP6 evaluation and projection of temperature and precipitation over China. *Advances in Atmospheric Sciences* **38**: 817–830. DOI: 10.1007/s00376-021-0351-4.

Ziehn T, Chamberlain M, Lenton A, Law R, Bodman R, Dix M, Wang Y, Dobrohotoff P, Srbinovsky J, Stevens L, Vohralik P, Mackallah C, Sullivan A, O'Farrell S, Druken K. 2019. CSIRO ACCESS-ESM1.5 model output prepared for CMIP6 CMIP historical. Version 20220607. *Earth System Grid Federation*. DOI: 10.22033/ESGF/CMIP6.4272.